Renewable Energy 146 (2020) 181–187

Contents lists available at ScienceDirect

Renewable Energy

journal homepage: www.elsevier.com/locate/renene

Experimental validation of the power enhancement of a pair of vertical-axis wind turbines

Antoine Vergaerde [a], Tim De Troyer [a, *], Lieven Standaert [a], Joanna Kluczewska-Bordier [b], Denis Pitance [b], Alexandre Immas [b, c], Frédéric Silvert [b], Mark C. Runacres [a]

[a] Vrije Universiteit Brussel, Pleinlaan 2, 1050, Brussels, Belgium
[b] Nenuphar, 1, rue du Professeur Calmette, 59000, Lille, France
[c] University of California, Berkeley, 6141 Etcheverry Hall, Berkeley, CA, 94720-1740, USA

ARTICLE INFO

Article history:
Received 13 August 2018
Received in revised form
11 May 2019
Accepted 20 June 2019
Available online 24 June 2019

Keywords:
Vertical-axis wind turbine
Paired wind turbines
Wind tunnel experiments

ABSTRACT

Wind tunnel tests have been performed of individual and paired H-type Darrieus vertical-axis wind turbines. The turbines in the paired configuration are closely spaced, at 1.2 and 1.3 rotor diameters shaft to shaft, and are counter-rotating. Two directions of rotation were studied, one where the facing (inner) blades move along with the incoming flow, and one where the facing blades move against the wind. The wind tunnel tests confirm a net increase in the power coefficient of the paired configuration compared with twice the power coefficient of the individual turbine. We found average relative increases in the power coefficients between 13% and 16%, which is consistent with numerical studies available in the literature.

1. Introduction

Vertical-axis wind turbines (VAWTs) were first thoroughly studied in the nineteen seventies and eighties under the impulse of Sandia National Laboratories. The review article from 2012 by Sutherland et al. [1] provides an overview of VAWT technology up to 1994, and concludes with an outlook on the future. Today, it is mainly with off-shore applications in mind that VAWTs are being considered as a viable alternative for horizontal-axis wind turbines (HAWTs), see e.g. Borg et al. [2] or Paulsen et al. [3]. One important driver for the renewed research interest certainly is the work by Dabiri and his co-workers (see i.a. [4–7]). They showed that closely-spaced VAWTs can have a mutually beneficial effect on the power output when compared to an individual VAWT.

In this article, we study the increase of the power coefficient for a side-by-side pair of VAWTs. In off-shore applications, it makes sense to place two counter-rotating VAWTs on one floating platform. Apart from the increase in power coefficient, such a setup would benefit from a zero net generator torque on the platform and a means (by varying the individual torque of each turbine) to change the orientation of the platform. This is important, as a side-by-side pair of VAWTs is dependent on the direction of the incoming wind, contrary to an individual VAWT. Through the same mechanism, it becomes possible to control the deflection of the wake of the pair, which could be used to divert the wake away from downstream turbines.

The increase of the power coefficient of VAWTs placed in close proximity, was originally studied by Schatzle et al. [8] and Rajagopalan et al. [9]. Dabiri [4] used field measurements to study this interaction. The positive effects on the power coefficient have been confirmed numerically by Duraisamy and Lakshmin–arayan [10], Zanforlin and Nishino [11] and Parneix et al. [12].

Most of the experimental studies on VAWTs so far have been focused on individual VAWTs. The seminal studies at Sandia on individual VAWTs are well known [13–16]. Other, more recent experimental work has been done on aerofoil design for VAWT applications [17], on the difference between the testing of VAWTs in confined and unconfined environments [18], on the impact of testing at low Reynolds numbers [19], and on the wake development behind a VAWT [20]. Also the use of flow control techniques has been considered [21–24].

To the authors' knowledge, the only wind tunnel study that

* Corresponding author Vrije Universiteit Brussel, Department of Engineering Technology, Pleinlaan 2, 1050, Brussels, Belgium.
E-mail addresses: antoine.vergaerde@vub.be (A. Vergaerde), tim.de.troyer@vub.be (T. De Troyer), lieven.standaert@vub.be (L. Standaert), jkb@bordier.eu (J. Kluczewska-Bordier), dpitance@gmail.com (D. Pitance), alexandre.immas@berkeley.edu (A. Immas), frederic.silvert@gmail.com (F. Silvert), mark.runacres@vub.be (M.C. Runacres).

https://doi.org/10.1016/j.renene.2019.06.115
0960-1481/

exists for multiple VAWTs (arrays of two and three turbines) is by Ahmadi-Baloutaki et al. [25]. However, these turbines had a very high solidity and were spaced well apart (2 diameters shaft to shaft), so the results are difficult to compare with the numerical studies available [10,11]. Therefore, the main focus of this article is on wind tunnel experiments of a pair of counterrotating H-type Darrieus VAWTs at very small inter-turbine distances (1.2 and 1.3 diameters shaft to shaft), to validate the power enhancement predicted by the numerical simulations.

The structure of this article is as follows. We first discuss the experimental setup used and the measurement procedure for the power output of the turbines. We then compare the performance of a single VAWT and a pair of VAWTs at different tip-speed ratios and inter-turbine distances and discuss the findings. Finally, the conclusions are drawn.

2. Experimental setup

2.1. VAWT rotor

The rotor is a two-bladed H-type Darrieus turbine with two NACA 0018 blades and two inclined struts per blade. The struts are slightly thicker (NACA 0024) for structural reasons. The rotor solidity, $\sigma = bc/D$, is 0.20, where b is the number of blades and D the rotor diameter. The chord length, c, is 50 mm. Fig. 1 shows the rotor and the setup with the rotor diameter and height, H, indicated with their respective symbol.

Given the small size of the rotor (set by the wind tunnel dimensions, see Section 2.4), high angular speeds (up to 1400 rpm) are required to achieve realistic tip-speed ratios (between 2 and 4) within the range of speeds at which can be tested in the wind tunnels (angular speed control is further discussed in Section 2.2). To withstand the centrifugal loads, the rotors were made in carbon-epoxy composite. The mass of one individual blade is only 181 g, for the struts it is 35 g each.

We performed a dynamic crash test, during which the rotor was gradually spun up until failure. The angular speed at which the rotor failed was just over 2100 rpm (219.9 rad/s), which ensures ample margin for the maximum speed anticipated during the wind tunnel tests.

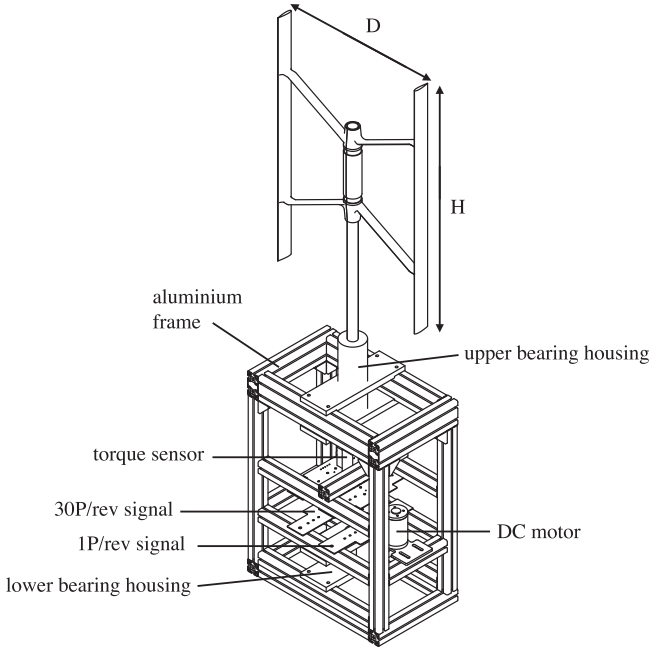

Fig. 1. A sketch of the general assembly of one VAWT rotor and its aluminium box that holds the torque sensor, drive belt, motor/generator, and peripherals.

2.2. Turbine housing and measurement equipment

The VAWT rotor is connected via a torque sensor and a drive belt (with gear ratio 100 /28) to a brushed-DC motor. This motor is used to drive the VAWT rotor during start-up and as a generator in normal operation. The electrical output of the motor is fed to a circuit with variable resistance for angular speed control and for measurement of the electrical power (through voltage and current measurements). This set-up provides adequate speed control while allowing sufficient freedom to let the VAWT rotors interact in paired operation.

We used a Lorenz Messtechnik DR-3000 torque sensor to measure mechanical torque and angular speed (and thus mechanical power) of the VAWT. It is fitted between two torsionally-stiff couplings to correct for possible misalignments. A one-pulse-per-revolution signal was acquired to compare the relative phase differences between interacting turbines. The torque sensor, drive belt, DC motor, and measurement equipment are housed inside an aluminium frame, as is shown in Figs. 1 and 2.

2.3. Set-up of the interaction tests

Two identical turbine housings with their respective measurement equipment are used for interaction tests. These two housings are placed within a larger aluminium frame (observable in Fig. 2). This structure is placed perpendicular to the incoming wind so that the turbines are placed side by side with regard to the flow. It is possible to vary the inter-turbine distances with this experimental setup.

Before proceeding to wind tunnel tests of the paired configuration, the performance of each rotor is measured individually to assure equal performance.

For all interaction tests, the directions of rotation of the rotors were opposite to each other. Two configurations have been tested, one where the facing (inner) blades move along with the incoming wind, and one where the facing blades move against the wind (Fig. 3). For clarity, we refer to these configurations as downwind-inner and upwind-inner respectively.

Fig. 2. The two turbines were placed in their respective frames in the assembly. A floating floor was mounted on top of the boxes.

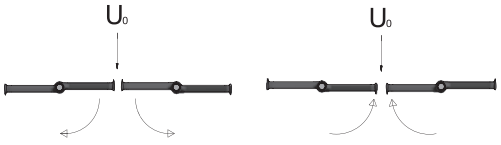

Fig. 3. Left: downwind-inner configuration; the facing (inner) blades move along with the incoming wind. Right: upwind-inner configuration; the facing (inner) blades move against the incoming wind.

2.4. Wind tunnel

Four different wind tunnels have been used to perform the experiments that are described in this article. Preparatory work was performed in the Vrije Universiteit Brussel's low-speed wind tunnel (VUB LS). This is a blow-down open-return wind tunnel with a rectangular, closed test section. It has a cross section of 2 m by 1 m and a length of 12 m. Tests were performed between 8 m/s and 12 m/s with an incoming turbulence intensity, TI, of 0.5%. These tests served to optimise the design of the experimental setup.

Further testing was performed in two open-jet wind tunnels, the OJF of the Delft University of Technology and the L1-A of the von Karman Institute for Fluid Dynamics (VKI). Both tunnels have a jet nozzle of 3 m diameter; the OJF is octagonal while the L1-A is circular. The free jet section is 4.5 m long for the L1-A and up to 13 m for the OJF. The turbulence intensity levels were around 0.3%. The objective of these tests was to measure the power coefficient of the rotor models as a function of tip-speed ratio and Reynolds number.

Final testing to analyse various configurations of paired VAWTs (inter-turbine spacing and direction of rotation) was performed in the GVPM of the Politecnico di Milano (PoliMi). This is a closed-circuit wind tunnel, arranged in a vertical layout with two test rooms in the loop. We used the low-speed test section with a cross section of 13.8 m by 3.8 m and a useable length of 12 m (the total length is 35 m). As the solid blockage ratio was only 2%, no blockage corrections have been applied. The turbulence intensity of the wind tunnel is 2%.

Table 1 summarizes the main characteristics of the used wind tunnel facilities. The wind tunnel width, height and maximum velocity are denoted with the symbols W_t, H_t and $U_{\max}$, respectively. The effective blockage ratio, ε (defined as the ratio of solid blockage induced by the setup to the cross section or jet size of the wind tunnel), is also included in this table. Note that the part of the turbine housing which is exposed to the flow differs for the different used facilities.

3. Measurement procedure for turbine power output

3.1. Power coefficient and tip-speed ratio

The mechanical power output of every turbine is individually measured and logged through the (rotating) torque sensor.

The power coefficient, C_P, is calculated from the mechanical torque, τ, and the angular speed, ω,:

$$C_P = \frac{P_{\text{mech}}}{P_{\text{wind}}} = \frac{\tau\omega}{\frac{1}{2}\rho D H U_0^3}, \tag{1}$$

where the power in the wind, P_{wind}, is calculated from the unperturbed wind tunnel speed, U_0, the air density, ρ, and the frontal swept area of the turbine, height, H, times diameter, D, which are indicated on Fig. 1. The unperturbed wind tunnel speed was typically measured using pitot-static tubes in front of the VAWT rotors. The wind speed and angular speed are combined into the tip-speed ratio, λ, defined as:

$$\lambda = \frac{\omega(D/2)}{U_0}. \tag{2}$$

3.2. Data reduction

The torque sensor measures angular speed and mechanical torque at a sample frequency of 2.5 kHz. The first step in the data reduction process was to calculate a (centred) running average over a 1-s period. This 1-s period corresponds to about 15–25 rotations of the turbine, which we found to be a good compromise between sufficient time resolution for post processing and reducing the noisiness of the data.

The next step in the data reduction was the identification of relatively long periods of time during which the angular speed remained sufficiently constant. These periods are referred to as *plateaus* in the remainder of the article. Different criteria were applied to identify a plateau: the standard deviation of the angular speed (calculated as the square root of a running variance over 40s periods) throughout the plateau should be less than $\sqrt{10}$ rpm. Moreover, the plateau should last at least 10s, and the slope of the plateau should be less than 0.05 rpm/s. These cut-off values were determined experimentally, to provide a good compromise between rejecting transient behaviour and including steady state data in the plateaus.

For turbines in paired configuration, an additional constraint was formulated: the angular speeds of the two turbines should be within 10% of one another. This constraint ensures that the turbines were indeed properly synchronised throughout a plateau.

Finally, the angular speed and mechanical power were averaged for every plateau and used to calculate the power coefficient (Eq. (1)) and tip-speed ratio (Eq. (2)). Also, the standard deviations of torque, angular speed, wind speed, and density, over the plateau were calculated, and then used (via the standard error propagation techniques) to derive the standard deviation on the power coefficient and tip-speed ratio. These standard deviations have been inserted as error bars in the figures containing experimental data (except for Fig. 6 to avoid overcrowding the figure) to represent the variations within every individual plateau.

3.3. Systematic errors

This experimental study is subjected to different sources of

Table 1
General characteristics of the used wind tunnel facilities.

Name	Type	Test section ($W_t \times H_t$) [m]	Cross section	TI [%]	$U_{\max}$ [m/s]	ε
VUB LS	blow-down	2×1	rectangular	0.5	20	0.40
OJF	open-jet	2.85×2.85	octagonal	0.3	35	0.11
L1-A	open-jet	3×3	circular	0.3	60	0.12
GVPM	closed-circuit	13.8×3.8	rectangular	2	16	0.02

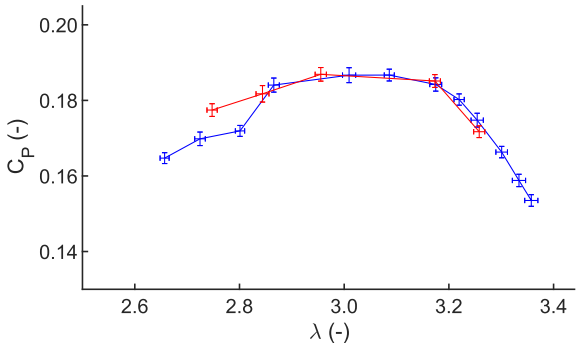

Fig. 4. curve of the best matching turbines in isolated configuration in the GVPM wind tunnel. The error on C_P and λ are represented by the vertical and horizontal error bars respectively. The figure serves as a reference case for comparison with the tests of a pair of turbines. Rotor 1 is shown in blue, rotor 2 in red. (For interpretation of the references to colour in this figure legend, the reader is referred to the Web version of this article.)

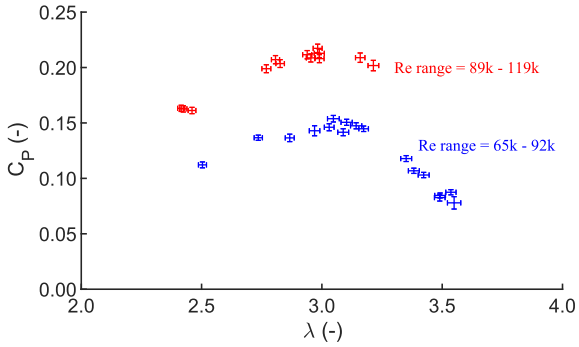

Fig. 5. Power coefficient as a function of tip-speed ratio and Reynolds number. The tests were performed at a constant wind speed: 7 m/s for the blue markers and 11 m/s for the red markers. The average Reynolds number thus varies proportional to the tip-speed ratio in these graphs. These tests were performed in the OJF and L1-A wind tunnels. (For clarity, the error bars here indicate twice the standard deviation.). (For interpretation of the references to colour in this figure legend, the reader is referred to the Web version of this article.)

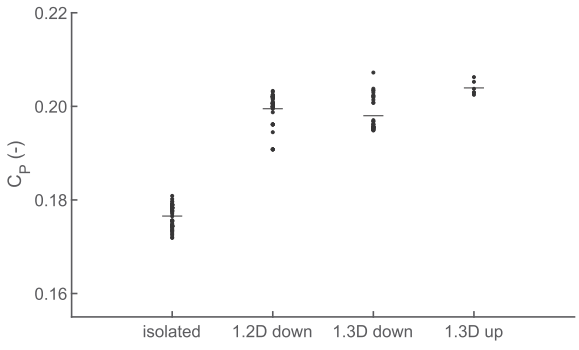

Fig. 6. Power coefficient near optimum tip-speed ratio for two inter-turbine distances with the same direction of rotation (downwind-inner) and an individual rotor. The standard error of the mean is included in Table 2. Error bars have been left out for clarity.

systematic errors, e.g. blockage effects, fluctuations of the wind speed and friction losses in the drive train. There is still debate on how to properly correct VAWT wind tunnel experiments for blockage [18]. As the solid blockage ratio of our pair of turbines in the GVPM was only 2%, no corrections were applied here. Furthermore, the preliminary tests in the open-jet facilities (data of those tests are only shown in Fig. 5) yielded almost identical circumstances and were only used for a relative comparison, obviating the need for an elaborate blockage correction. On the other hand, fluctuations in the wind speed are pertinent and necessitate a proper correction. These fluctuations are specifically taken into account in the data reduction process and are an important element of the overall error on the power coefficients and tip-speed ratios.

A correction for the torque losses induced by the drive train is determined by utilizing the generator as a motor to impose a rotation without rotor. This way, the torque sensor only measures a net torque due to frictional losses in the drive train. We found that the measured torque losses increase proportionally over the operating range of the rotors from 2.9cNm to 3.4cNm. All experimental power coefficients further presented in this study have been corrected for torque losses in the drive train according to their corresponding angular speed.

4. Results

4.1. The power production of isolated VAWTs

Several rotors were manufactured and tested individually in the wind tunnels at different wind speeds and tip-speed ratios. Because of the small size of the rotors, small manufacturing deficiencies resulted in different performance characteristics of the manufactured rotors. Two rotors, of which the maximum power coefficient differs less than one standard deviation, were selected for the interaction tests. Fig. 4 shows the $C_P(\lambda)$ curve with corresponding errors of these two rotors. The curves match, except at tip-speed ratios well below the optimum. The rather abrupt increase in power coefficient between tip-speed ratios 2.8 and 2.9 exhibited by rotor 1 (the blue curve in Fig. 4), is related to an unstable operating regime caused by a structural resonance of the rotor. Because the generator back torque had to be increased during the speed up of the rotor from a tip-speed ratio of 2.8–2.9, the corresponding increase of power over this range of tip-speed ratios is artificially high and not only related to aerodynamics. Also the second rotor (the red curve in Fig. 4) exhibited an unstable operating region, but at a lower tip-speed ratio (below 2.7). This region is not shown on Fig. 4, as for rotor 2, individual measurements were only performed at these low angular speeds during preparatory testing. The difference in the location of the unstable region is also related to differences in friction in the respective drive trains, and thus a difference in the variation of the back torque as a function of angular speed.

4.2. Effect of the Reynolds number

To appraise the sensitivity of our experiments to variations in the Reynolds number, we measured power coefficients for a combination of angular speeds of the rotor and wind tunnel speeds. From momentum theory, one would expect a fixed power coefficient for a given tip-speed ratio. Changes in power coefficient at a given tip-speed ratio are likely to be caused by Reynolds number effects [26].

Of course, the blade Reynolds number (based on the chord length, c) varies throughout one revolution. The speed a blade sees varies roughly between $(\lambda - 1)U_0$ and $(\lambda + 1)U_0$, if induction is neglected. For ease of comparison, we define an average Reynolds number, $\overline{\mathrm{Re}}$, which is based on the average circumferential speed, $\omega(D/2) = \lambda U_0$:

$$\overline{\mathrm{Re}} = \frac{c\lambda U_0}{\nu}, \tag{3}$$

where ν is the kinematic viscosity of air.

Fig. 5 shows a set of measurements of the power coefficient at two different wind speeds and a range of angular speeds. For both tests, the wind speed was kept constant and the angular speed was varied. As a result, $\overline{\mathrm{Re}}$ varies proportionally to the tip-speed ratio.

Two interesting conclusions can be noted.

1. The maximum obtained power coefficient is larger for the higher $\overline{\mathrm{Re}}$: it evolves from 0.15 at $\overline{\mathrm{Re}} \approx 80000$ to 0.22 at $\overline{\mathrm{Re}} \approx 110000$. This increase can be attributed to the higher lift-to-drag ratio of the blades at higher $\overline{\mathrm{Re}}$ (for the same angles of attack).
2. The optimum tip-speed ratio at which the maximum power is obtained, is slightly higher for the lower $\overline{\mathrm{Re}}$. This is probably related to the fact that, for our measurements at a fixed wind speed, a higher tip-speed ratio corresponds to a higher $\overline{\mathrm{Re}}$. Thus, the drop in power coefficient beyond the theoretically optimum tip-speed ratio will initially be offset by an increase in the lift-to-drag ratio related to the increase in $\overline{\mathrm{Re}}$.

These findings follow the same trend as the data in Fig. 5 of [26].

As a compromise between average Reynolds number and angular speed (to limit the centrifugal loads), the interaction tests are performed at a wind tunnel speed of 10.6 m/s. In this case, given that the optimum tip-speed ratio is close to 3, $\overline{\mathrm{Re}} \approx 110000$ as calculated with Eq. (3).

4.3. The definition of VAWTs in interaction

To study the power output of a pair of VAWTs, the power coefficient is redefined as the simple average of the two individual power coefficients:

$$\overline{C}_P = \frac{P_1 + P_2}{\frac{1}{2}\rho U_0^3 (2DH)} = \frac{1}{2}\left(C_{P,1} + C_{P,2}\right). \tag{4}$$

where the index refers to the individual rotors.

Before every test, the rotors are homed to a fixed position with the plane of the rotor perpendicular to the incoming wind. Then, the rotors are spun up individually to the desired angular speed and brought to within about 20 rpm of each other (±2%). We observed that the rotors tend to synchronise spontaneously: the angular speeds equalise, and the phase difference between both rotors remains constant, with the inner blades passing each other approximately as shown in Fig. 3.

To ensure consistency in the comparison between the different tests, all interaction tests that are presented in this article have been performed with the rotors synchronised.

4.4. The power increase of interacting VAWTs

To measure the increase of the power coefficients for a pair of interacting VAWTs, the rotors were operated in synchronisation near maximum C_P for different inter-turbine spacings and directions of rotation. The baseline configuration in interaction is with the hubs spaced 1.3D apart and with the turbines in the downwind-inner configuration. Then two more configurations were tested and compared with the baseline:

- downwind-inner, with now the hubs spaced 1.2D apart,
- upwind-inner, with the hubs again spaced 1.3D apart.

Every configuration was tested until at least 120min of plateaus were measured. (This duration was determined by wake measurements that were done simultaneously; it provided ample data to make reliable estimates of the power coefficients.) Table 2 shows, per configuration, the average values and standard deviations of the power coefficient and tip-speed ratio for these tests. (The average is an unweighted average over all the identified plateaus that were measured in a specific configuration and at the optimum tip-speed ratio.) For the tests with a pair of VAWTs, also the average of the power coefficient (using Eq. (4)) was calculated, as well as the corresponding standard error of the mean.

With respect to the individual-VAWT C_P of 0.176, a pair of VAWTs spaced 1.3D apart in the downwind-inner configuration experiences an average increase in C_P of 0.023 (13.1%). This increase is in agreement with the 12.6% increase observed by Zanforlin and Nishino [11] in their Figure 11 for a pair of 1.5D spaced VAWTs (which is the closest distance they considered), or the 11% increase calculated by Parneix et al. [12] in their Figure 10 (also at a spacing of 1.3D). The increase in power we measure is seen by both rotors, slightly more by rotor 1 (up 0.025) than by rotor 2 (up 0.021).

Then, when the turbines are placed closer, at 1.2D apart, but still in the same downwind-inner configuration, the average increase in power coefficient is a little more than at 1.3D apart (up 0.024, or 13.6%), and also the standard deviation has slightly increased. However, given that the standard deviation is 0.003, we cannot conclude that the difference in *average* power enhancement between turbines at 1.2D and 1.3D is statistically significant. Fig. 6 compares the power coefficients (calculated at all the identified plateaus) for both inter-turbine distances and both directions of rotation with those of the individual rotor. We found that the relatively weak increase when going from 1.3D to 1.2D is caused by a small number of plateaus where the rotors exhibited a lower power output than usual (see the bottom three dots for 1.2D 'down' in Fig. 6, and compare the average power coefficients for rotor 1 (0.204) and rotor 2 (0.197) in Table 2). With these plateaus left out, the average power coefficient at 1.2D increases to 0.201, with rotor 1 at 0.206 and rotor 2 at 0.198. However, as no specific anomalies could be detected during the processing of these measurements, we have included the data in the figures and the table.

When the turbines were tested in the upwind-inner configuration (again 1.3D apart), we found a more significant increase in the average maximum power coefficient (from 0.176 to 0.204, which corresponds to 15.9%) when compared with the isolated turbine (see Table 2). This increase in power coefficient is larger than the numerical results of Zanforlin and Nishino [11], who predict an increase of only about 7% for the upwind-inner configuration (but again at a distance of 1.5D). Experimentally, we observed that the synchronisation between the two turbines was stronger for the upwind-inner configuration than for downwind-inner: the fluctuations of the phase difference (see Section 4.3)

Table 2
Average power coefficient for different configurations obtained during long-duration testing near the tip-speed ratio for optimum C_P. The S represents the standard error of the mean.

Configuration	λ	S_λ	$C_{P,11}$	$S_{C_{P,11}}$	$C_{P,12}$	$S_{C_{P,12}}$	$C_{P,\mathrm{mean}}$	$S_{C_{P,\mathrm{mean}}}$
Isolated turbine	2.992	0.001	0.176	0.0004	(−)	(−)	(−)	(−)
Downwind-Inner, 1.3D	3.079	0.001	0.201	0.0009	0.197	0.0007	0.199	0.0008
Downwind-Inner, 1.2D	3.097	0.003	0.204	0.0006	0.197	0.0006	0.200	0.0006
Upwind-Inner, 1.3D	3.081	0.004	0.202	0.0013	0.206	0.0008	0.204	0.0011

had a magnitude which was 70% smaller for the upwind-inner configuration than for the downwind-inner configuration. Also, it required a more asymmetric loading of the generators to break the synchronisation. This is also reflected in Fig. 6, by comparing between the two directions of rotation (upwind-inner vs. downwind-inner) at 1.3*D* apart. For the upwind-inner configuration, clearly less plateaus were identified, but each plateau was of a longer duration, confirming the more stable synchronisation.

4.5. VAWT interaction at off-design tip-speed ratios

To also study the effect of interaction at tip-speed ratios away from the optimum, we simultaneously varied the angular speed of both rotors to measure the power output for different plateaus. Fig. 7 provides a comparison between our experimental data and the simulations of Zanforlin and Nishino [11]. The power coefficients have been rescaled with the maximum C_P of the isolated turbine, while the tip-speed ratios have been shifted to set the tip-speed ratio corresponding to the maximum C_P at zero. A number of interesting conclusions can be drawn from this comparison.

1. The increase in power coefficient is evident in both the numerical and experimental data (compare the isolated configuration in blue with interaction in red and green). Moreover, this increase clearly persists before and after the optimum tip-speed ratio. (The fact that the increase in power coefficient is of the same order of magnitude for the experimental and numerical data, however, should not be overly interpreted. Differences in setup such as the absence of shaft, struts or blade tip effects in the simulations do not warrant this.)
2. The tip-speed ratio at which maximum C_P is reached, is higher for turbines in interaction than the optimum tip-speed ratio for an isolated turbine. This was shown numerically by Zanforlin and Nishino [11] and is confirmed here.
3. The shapes of the curves are different for experiments and simulations. The experimental data exhibit a rather flat optimum (it is rather a range of tip-speed ratios where maximum C_P is obtained), while the optimum in the numerical data is sharper. The difference at high tip-speed ratios is most pronounced. The increase in negative torque due to drag of the struts at high tip-speed ratios is thought to cause the rather sharp drop in C_P that we measured experimentally (No struts were considered in Ref. [11].). At tip-speed ratios below the optimum, the difference in C_P is smaller. These differences are most probably related to the presence of dynamic stall and how it affects the instantaneous lift and drag forces on the blades.

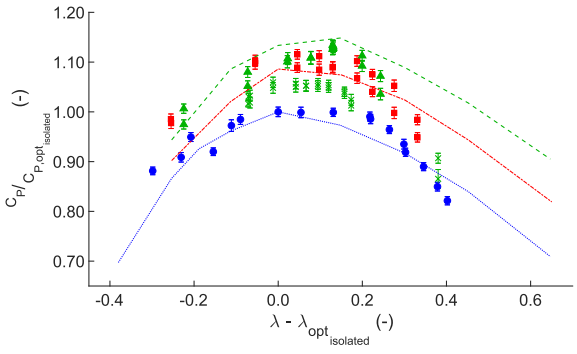

Fig. 7. Power curves for the different configurations tested. The numerical data from Zanforlin and Nishino [11] (their Figure 11) is shown by lines, while the present (experimental) data is only shown by markers. Blue (dotted line, dots) are the power coefficients for an isolated configuration, red (dash-dotted line, squares) are for the upwind-inner rotating configuration, green (dashed, triangles and crosses) are for the downwind-inner rotating configuration. The numerical data were obtained for a spacing of 1.5*D* between the turbines, while the experimental data were at 1.3*D* (squares and crosses) and 1.2*D* (triangles) respectively. The power coefficients have been rescaled with the maximum C_P of the isolated turbine, while the tip-speed ratios have been shifted to set the tip-speed ratio corresponding to the maximum C_P at zero. The error of C_P is indicated with vertical error bars, while the error on λ is around the same size of the used markers and left out for clarity. (For interpretation of the references to colour in this figure legend, the reader is referred to the Web version of this article.)

4.6. Aerodynamic interpretation of the power enhancement

Based on their numerical simulations, Zanforlin and Nishino [11] attribute the power increase of paired counter-rotating VAWTs to two physical mechanisms:

1. A more favourable incident angle of the incoming wind caused by the upwind influence of the blockage induced by a neighbouring turbine,
2. A wake contraction in the downwind path.

In this experimental study, no wake measurements are included but it is possible to interpret the power improvement based on the first physical mechanism.

For an isolated turbine configuration, the local flow around the turbine is skewed because of the blockage induced by the turbine. This skew is counteracted on one side of the turbine by placing another turbine closely. It is this counteraction of the local flow skew that results in a more favourable incoming wind direction. This means that the more beneficial flow angle mostly influences the inner-moving blades, i.e. the blades closest to the centreline perpendicular to the wind direction. For the downwind-inner and upwind-inner configuration, the position of the upwind moving blade is respectively at the outer sides and at the inner sides of the pair. This suggests that the advantage of a more favourable incoming flow angle is biggest for the upwind-inner configuration, and that is indeed confirmed in Table 2.

Admittedly, the average Reynolds number for this study is around 110 000, which is relatively low, but comparable to or higher than other experimental studies currently available ([4,25] respectively). How these findings can be extrapolated to higher Reynolds numbers, is hard to predict accurately. As the benefit of pairing counter-rotating VAWTs seems to originate mainly from geometric characteristics of the flow, we expect this effect to persist at higher Reynolds numbers. However, a precise estimate of the relative increase in power is beyond the scope of this study.

Finally, it should be noted that the substantial rise of the power coefficients in paired operation implies a corresponding increase of the overall loads on the rotor. Though it was not separately measured in this campaign, the average normal and tangential aerodynamic forces on the blades can be expected to increase proportionally with the increased torque load on the drive train. Of course, this increase should be taken into account when designing VAWT rotors specifically for paired operation.

5. Conclusions

Wind tunnel experiments have been used to analyse the performance of a pair of two H-type Darrieus VAWTs placed side-by-side in close vicinity in a plane normal to a uniform inflow. For small inter-turbine distances (1.2 and 1.3 times the rotor diameter), we observed a power increase of up to about 16% for a pair of VAWTs compared with two individual VAWTs. Apart from the distance between the turbines, the power increase also depends on the tip-speed ratio and the direction of rotation.

Two directions of rotation were studied, one where the facing (inner) blades move along with the incoming wind, and one where the facing blades move against the wind. Both configurations showed clear power increases and synchronisation behaviour, but the increase was more pronounced for upwind-inner case (16% versus 13%), where the facing (inner) blades are moving against the incoming wind.

The power coefficient curve (as a function of tip-speed ratio) for a pair of VAWTs seems to flatten compared with the curve for an individual VAWT. It seems that the mutual interaction (in a synchronised state) is so stable that a pair can keep producing near-optimum power over a larger range in tip-speed ratios than for an individual VAWT.

Our wind tunnel experiments validate the numerical predictions of the increase in power coefficient for a pair of closely-spaced interacting H-Darrieus VAWTs.

Declarations of interest

None.

Acknowledgements

The authors would like to thank the technical staff of the wind tunnels we used at the Vrije Universiteit Brussel, the Technische Universiteit Delft, the von Karman Institute for Fluid Dynamics, and the Politecnico di Milano. In particular, the support from Marco Belloli, Ilmas Bayati, Carlos Simão Ferreira, Simon Horb, Bruce LeBlanc, Nicolas Parneix, Luca Ronchi, and Alain Wery, is gratefully acknowledged. The financial support of Nenuphar and of the department of Engineering Technology is acknowledged. The authors would also like to thank the master students Evert Van Geite, Ruben De Smet, and Laurent Gutty, who built and tested early versions of the setup.

References

[1] H.J. Sutherland, D.E. Berg, T.D. Ashwill, A Retrospective of VAWT Technology, Tech. Rep. SAND2012-0304, Sandia National Laboratories, 2012.
[2] M. Borg, A. Shires, M. Collu, Offshore floating vertical axis wind turbines, dynamics modelling state of the art. Part I: Aerodynamics, Renew. Sustain. Energy Rev. 39 (1214–1225) (2014). ISSN 1364-0321.
[3] U.S. Paulsen, H.A. Madsen, J.H. Hattel, I. Baran, P.H. Nielsen, Design optimization of a 5 MW floating offshore vertical-axis wind turbine, Energy Procedia 35 (22–32) (2013). ISSN 1876-6102.
[4] J.O. Dabiri, Order-of-magnitude enhancement of wind farm power density via counter-rotating vertical-axis wind turbine arrays, J. Renew. Sustain. Energy 3 (2011), 043104.
[5] R.W. Whittlesey, S. Liska, J.O. Dabiri, Fish schooling as a basis for vertical axis wind turbine farm design, Bioinspiration Biomimetics 5 (3) (2010). ISSN 1748-3182.
[6] M. Kinzel, Q. Mulligan, J.O. Dabiri, Energy exchange in an array of vertical-axis wind turbines, J. Turbul. 13 (1) (2012).
[7] J.O. Dabiri, R.W. Whittlesey, Two-dimensional Array of Turbines, US Patent US8545168B2, 2013.
[8] P. Schatzle, P.C. Klimas, H. Spahr, Aerodynamic interference between two Darrieus wind turbines, J. Energy 5 (2) (1981) 84–88.
[9] R.G. Rajagopalan, P.C. Klimas, T.L. Rickerl, Aerodynamic interference of vertical axis wind turbines, J. Propuls. Power 6 (5) (1990) 645–653.
[10] K. Duraisamy, V. Lakshminarayan, Flow physics and performance of vertical Axis wind turbine arrays. AIAA Applied Aerodynamics Conference, 2014.
[11] S. Zanforlin, T. Nishino, Fluid dynamic mechanisms of enhanced power generation by closely spaced vertical axis wind turbines, Renew. Energy 99 (2016) 1213–1226.
[12] N. Parneix, R. Fuchs, A. Immas, F. Silvert, P. Deglaire, Efficiency improvement of vertical-axis wind turbines with counter-rotating lay-out. Proceedings of the EWEA Annual Event, 2016.
[13] R.E. Akins, D.E. Berg, W.T. Cyrus, Measurements and calculations of aerodynamic torques for a vertical-axis wind turbine. Tech. Rep. SAND86–2164, Sandia National Laboratories, 1987.
[14] R.E. Sheldahl, P.C. Klimas, L.V. Feltz, Aerodynamic Performance of a 5-Metre-Diameter Darrieus Turbine with Extruded Aluminum NACA-0015 Blades, 80–0179, Sandia National Laboratories, 1980.
[15] R.E. Sheldahl, Comparison of Field and Wind Tunnel Darrieus Wind Turbine Data, SAND80-2469, Sandia National Laboratories, 1981.
[16] R.E. Sheldahl, P.C. Klimas, Aerodynamic Characteristics of Seven Symmetrical Airfoil Sections through 180-degree Angle of Attack for Use in Aerodynamic Analysis of Vertical axis Wind turbines., Tech. Rep. SAND81-2114, Sandia National Laboratories, 1981.
[17] D. Ragni, C.S. Ferreira, G. Correale, Experimental investigation of an optimized airfoil for vertical-axis wind turbines, Wind Energy 18 (9) (2015) 1629–1643.
[18] V. Dossena, G. Persico, B. Paradiso, L. Battisti, S. Dell'Anna, A. Brighenti, E. Benini, An experimental study of the aerodynamics and performance of a vertical axis wind turbine in a confined and unconfined environment, J. Energy Resour. Technol. 137 (5) (2015), 051207.
[19] J. McNaughton, F. Billard, A. Revell, Turbulence modelling of low Reynolds number flow effects around a vertical axis turbine at a range of tip-speed ratios, J. Fluids Struct. 47 (2014) 124–138.
[20] D.B. Araya, J.O. Dabiri, A comparison of wake measurements in motor-driven and flow-driven turbine experiments, Exp. Fluid 56 (7) (2015) 150. ISSN 1432-1114.
[21] M. Benedict, V. Lakshminarayan, J. Pino, I. Chopra, Aerodynamics of a small-scale vertical-Axis wind turbine with dynamic blade pitching, AIAA J. 54 (3) (2016) 924–935.
[22] D. Greenblatt, M. Schulman, A. Ben-Harav, Vertical axis wind turbine performance enhancement using plasma actuators, Renew. Energy 37 (2012) 345–354.
[23] D. Greenblatt, R. Lautman, Inboard/outboard plasma actuation on a vertical-axis wind turbine, Renew. Energy 83 (2015) 1147–1156.
[24] D. Greenblatt, A. Ben-Harav, H. Mueller-Vahl, Dynamic stall control on a vertical-Axis wind turbine using plasma actuators, AIAA J. 52 (2) (2014) 456–462.
[25] M. Ahmadi-Baloutaki, R. Carriveau, D.S.-K. Ting, A wind tunnel study on the aerodynamic interaction of vertical axis wind turbines in array configurations, Renew. Energy 96 (2016) 904–913.
[26] M.A. Miller, S. Duvvuri, I. Brownstein, M. Lee, J.O. Dabiri, M. Hultmark, Vertical-axis wind turbine experiments at full dynamic similarity, J. Fluid Mech. 844 (2018) 707–720.